Cramer-Rao bounds for long-wave infrared gaseous plume quantification

Citation: Golowich, Steven E., and Dimitris G. Manolakis. "Cramer-Rao Bounds for Long-Wave Infrared Gaseous Plume Quantification." Opt. Eng 53, no. 2 (December 16, 2013): 021109. © 2014 SPIE

As Published: http://dx.doi.org/10.1117/1.oe.53.2.021109

Publisher: SPIE

Persistent URL: http://hdl.handle.net/1721.1/86021

Version: Final published version: final published article, as it appeared in a journal, conference proceedings, or other formally published context

Optical Engineering

SPIEDigitalLibrary.org/oe

Cramer-Rao bounds for long-wave infrared gaseous plume quantification

Steven E. Golowich
Dimitris G. Manolakis

Optical Engineering 53(2), 021109 (February 2014)

Cramer-Rao bounds for long-wave infrared gaseous plume quantification

Steven E. Golowich
Dimitris G. Manolakis
MIT Lincoln Laboratory
244 Wood Street
Lexington, Masachusetts 02420
E-mail: golowich@ll.mit.edu

Abstract. The central parameter in the quantification of chemical vapor plumes via remote sensing is the mean concentration-path length (CL) product, which can be combined with scene geometry information to provide estimates of the absolute gas quantity present. We derive Cramer-Rao lower bounds on the variance of an unbiased estimator of CL in concert with other parameters of a nonlinear radiance model. These bounds offer a guide to feasibility of CL estimation that is not dependent on any given algorithm. In addition, the derivation of the bounds yields great insight into the physical and phenomenological mechanisms that control plume quantification, which we illustrate with examples representing a variety of experimental scenarios. [DOI: 10.1117/1.OE.53.2.021109]

Subject terms: hyperspectral imaging; chemical plume quantification; long-wave infrared; performance bounds.

Paper 131185SSP received Aug. 1, 2013; revised manuscript received Oct. 21, 2013; accepted for publication Nov. 5, 2013; published online Dec. 16, 2013.

1 Introduction

The remote sensing of chemical vapor plumes via hyperspectral imaging in the long-wave infrared (LWIR) region has a wide variety of applications—for example, warning of hazardous airborne chemical agents due to deliberate or inadvertent release, regulation of industrial pollutants, or weapons production monitoring. There is a corresponding variety of possible sensor geometries as well as desired analysis products, which can be divided into the categories of detection of an anomalous gaseous plume, identification of its constituents, and quantification of the amounts. In this paper, we consider the problem of determining the fundamental performance limits of plume quantification and of the relative importance of the various determining factors.

The central parameter in plume quantification is the mean concentration-path length (CL) product. When combined with information about the sensor and scene geometry, such as instantaneous field of view and distance to the plume, estimates of CL enable recovery of absolute gas quantity in each pixel of a scene. For some applications, this ancillary information may be available for single scenes from an individual sensor. Alternatively, when the plume is viewed from more than one aspect with multiple sensors, tomographic reconstruction algorithms enable plume quantification from CL estimates. Additionally, CL plays a large role as the key nonlinear parameter in the radiance signal model through Beer's law. This nonlinear dependence is important when optically thick plumes are observed, and indeed in these cases, CL estimation can play a role in the detection and identification as well as quantification.

The goal of this paper is to obtain quantitative fundamental performance bounds that apply to a broad range of sensors, system architectures, scenes, and statistical algorithms, although we will restrict the discussion to imaging sensors.[1–3] We will derive Cramer-Rao lower bounds on the variance of unbiased estimators of CL in concert with other parameters of a common nonlinear radiance model. These bounds offer a guide to feasibility of CL estimation, given a set of sensor system parameters that is not dependent on any given algorithm. They provide a very useful tool for both system design and assessment, as the parameters of any useful system must lead to sufficiently low CR bounds. A fielded system may be evaluated on the basis of how closely the theoretical limits are approached.

Another reason to compute CR bounds is that the derivations themselves yield great insight into the physical and phenomenological mechanisms that control CL estimation. There are four physical mechanisms that play a role: nonlinearities in the plume transmittance, spectral structure in the background radiance, spatial variability in the background, and the relative temperatures of the plume, atmosphere, and background. The performance limits due to these factors are driven by interactions between the characteristics of the sensor, gases to be detected, and background radiance. The complexity of this interaction means that the quality of an estimate of CL may vary greatly within a single image. Specific CL estimation algorithms may take advantage of only one, or more than one, of these mechanisms, depending on the intended application.

2 Radiance Model

2.1 *Three-Layer Radiative Transfer*

The choice of an appropriate radiance model for gaseous plumes in the LWIR has been extensively studied.[4,5] The analysis of Sec. 4.1 will be carried out in the context of the widely used radiative transfer model with three parallel atmospheric layers orthogonal to the line of sight of the sensor. The first layer extends from behind the plume to the background; the second layer is the plume itself; and the third layer is the atmosphere between the plume and the sensor. Each layer attenuates the radiation that passes through it as well as emits radiation on the basis of its

0091-3286/2014/$25.00

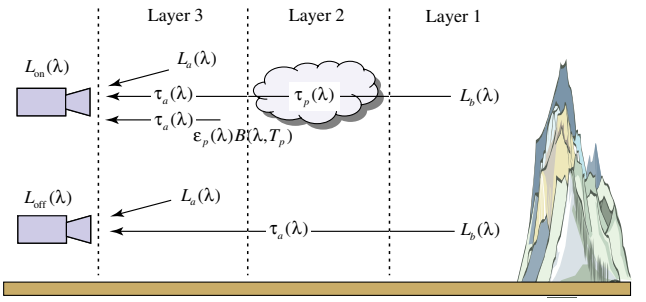

Fig. 1 Three-layer side-looking radiative transfer radiance signal model for standoff chemical agent detection.

own content and temperature. This is illustrated in Fig. 1 for a standoff sensor with horizontal line of sight.

Several simplifying assumptions are made to arrive at expressions for the at-sensor radiance in the absence and presence of the chemical plume. The atmosphere and plume are assumed free of aerosols and particulate matter, so that scattering may be neglected throughout. The thickness of the plume layer and the distance between the plume and background are assumed to be small enough so that the atmospheric transmittance in these layers may be neglected. The plume and atmosphere are each assumed homogeneous in both temperature and composition. Finally, downwelling radiance from both plume and atmosphere are neglected.

With these assumptions, the at-sensor radiance in the absence of plume, as a function of wavelength, is given by the radiative transfer theory[6] to be

$$L_{\text{off}}(\lambda) = [1 - \tau_a(\lambda)]B(\lambda, T_a) + \tau_a(\lambda)L_b(\lambda), \tag{1}$$

where the two terms represent atmospheric radiance and background radiance modulated by the atmosphere. In Eq. (1), $\tau_a(\lambda)$ is defined to be the atmospheric transmittance, T_a is the temperature of the atmosphere, $L_b(\lambda)$ is the background radiance, and $B(\lambda, T)$ is the Planck function evaluated at wavelength λ and temperature T

$$B(\lambda, T) = \frac{2\,hc^2}{\lambda^5}\frac{1}{e^{\frac{hc}{\lambda kT}} - 1}, \tag{2}$$

with h and k denoting the Planck and Boltzmann constants.

The presence of a plume has two effects: it absorbs part of the radiation emitted by the background and it emits its own radiation. The resulting radiance is subsequently attenuated by transmission through the atmosphere and is given by

$$\begin{aligned} L_{\text{on}}(\lambda) = {} & [1 - \tau_a(\lambda)]B(\lambda, T_a) + \tau_a(\lambda)\tau_p(\lambda)L_b(\lambda) \\ & + \tau_a(\lambda)[1 - \tau_p(\lambda)]B(\lambda, T_p), \end{aligned} \tag{3}$$

where $\tau_p(\lambda)$ is the plume transmittance and T_p its temperature. In Eq. (3), the three terms represent the at-sensor radiance due to the atmosphere, the background radiance as modulated by the plume and atmosphere, and the plume radiance as modulated by the atmosphere.

In practice, the spectra are observed at only a finite set of sample points $\{\lambda_i\}_{i=1}^{N_{\text{band}}}$ after convolution with the sensor point spread function $g(\lambda)$. The operation of convolution does not in general commute with that of taking products of spectrally varying functions, but it does commute to a very good approximation if one of the functions is spectrally smooth or if the functions are uncorrelated with each other.[7] We will assume that the plume gases are uncorrelated with those of the atmosphere, which allows us to represent the smoothed and sampled form of Eq. (3) by

$$\begin{aligned} \boldsymbol{L}_{\text{on}} = {} & (\mathbf{1} - \boldsymbol{\tau}_a)\odot\boldsymbol{B}(T_a) + \boldsymbol{\tau}_a\odot\boldsymbol{\tau}_p\odot\boldsymbol{L}_b \\ & + \boldsymbol{\tau}_a\odot(\mathbf{1} - \boldsymbol{\tau}_p)\odot\boldsymbol{B}(T_p) + \boldsymbol{n}, \end{aligned} \tag{4}$$

where a bold symbol, e.g., $\boldsymbol{f}$, represents a vector with components $f_i = f * g(\lambda_i)$, and the Hadamard product is denoted by $\odot$. In Eq. (4), we have also added a noise component $\boldsymbol{n}$, which represents all sources of sensor noise.

The form of the radiance expressions [Eqs. (1) and (3)] elucidate the physical origins of the various contributions, but are not the most convenient for further processing. The alternative mathematically equivalent form

$$[\boldsymbol{L}_{\text{on}} - (\mathbf{1} - \boldsymbol{\tau}_a)\boldsymbol{B}(T_a)]\odot\boldsymbol{\tau}_a^{-1} = \boldsymbol{B}(T_p) + \boldsymbol{\tau}_p\odot[\boldsymbol{L}_b - \boldsymbol{B}(T_p)] + \tilde{\boldsymbol{n}}, \tag{5}$$

is referred to as the atmospherically compensated form.[8] All dependence on the atmosphere is isolated on the left hand side, while the right hand side depends only on the plume and background properties. The compensated noise term is given by $\tilde{\boldsymbol{n}} = \boldsymbol{n}/\boldsymbol{\tau}_a$.

The spectral transmittance function, $\tau_p(\lambda)$, of a plume with M gas species can be modeled using Beer's law

$$\tau_p(\lambda) = \exp\left[-\sum_{m=1}^{N_{\text{gas}}}\gamma_m\alpha_m(\lambda)\right]. \tag{6}$$

The function $\alpha_m(\lambda)$, which is known as the absorption coefficient spectrum, is unique for each gaseous chemical and can be used as a spectral fingerprint. The quantity γ_m is the CL parameter and is the product of two terms: the length ℓ along the sensor boresight that represents the depth of the cloud and the average concentration C_m along that path. For simplicity, we will work with the approximation for the smoothed and sampled transmittance[9]

$$\boldsymbol{\tau}_p \simeq \exp\left(-\sum_{m=1}^{N_{\text{gas}}}\gamma_m\boldsymbol{\alpha}_m\right). \tag{7}$$

We note that the analysis below does not depend on Eq. (7) in any essential way and could be extended to a more accurate band model for $\boldsymbol{\tau}_p$.[10]

2.2 *Analysis Assumptions*

Given the radiance model [Eq. (5)], the CL estimation problem may be cast in the following form. The observed data are the radiances of the on- and off-plume pixels, $\boldsymbol{L}_{\text{on}}$ and $\boldsymbol{L}_{\text{off}}$. From this data, the CL parameters $\{\gamma_i\}_{i=1}^{N_{\text{gas}}}$ must be estimated, with nuisance parameters T_p, T_a, $\boldsymbol{L}_b$, $\boldsymbol{\tau}_a$, in the presence of measurement noise $\boldsymbol{n}$. The gas signatures $\{\boldsymbol{\alpha}_i\}_{i=1}^{N_{\text{gas}}}$ are obtained from a library.[11]

The goal of this paper is to compute performance bounds on CL estimators. To this end, we make several simplifying assumptions that are realistic but also optimistic, in the sense

that they lead to improved performance. First, we will work with only a single gas species in the plume. Second, we will assume that the segmentation problem of the hyperspectral image into the plume and background components has been accomplished without error. Third, we will assume that the atmospheric radiance and transmittance are constant over the entire image and have been estimated without error either via ancillary measurements or by in-scene estimation, using the background pixels. Fourth, we will take the sensor noise $\boldsymbol{n}$ to be mean-zero multivariate Gaussian and independent from pixel to pixel. Finally, we assume that the background radiance $\boldsymbol{L}_b$ is spectrally slowly varying as compared to the gas signatures. This final assumption allows us to represent $\boldsymbol{L}_b$ by the low-order subspace model.

$$\boldsymbol{L}_b = \boldsymbol{W}\boldsymbol{c}, \tag{8}$$

where $\boldsymbol{W}$ is an $N_{\text{band}} \times N_{\text{basis}}$ matrix of basis functions and c is an N_{basis}-dimensional vector of expansion coefficients. In the examples below, we will use a B-spline expansion, although other choices would be equally valid.

These assumptions allow us to cast the radiance model in a form that is more amenable to analysis of the CL estimation problem. The raw data may now be taken to be the compensated radiances.

$$\boldsymbol{L}^{(\text{comp})} = [\boldsymbol{L} - (\boldsymbol{1} - \boldsymbol{\tau}_a)\odot\boldsymbol{B}(T_a)]\odot\boldsymbol{\tau}_a^{-1}. \tag{9}$$

With Eq. (8), our simplified radiance model is

$$\boldsymbol{L}_{\text{on}}^{(\text{comp})} = \boldsymbol{W}\boldsymbol{c} + (\boldsymbol{1} - e^{-\gamma\boldsymbol{\alpha}})\odot[\boldsymbol{B}(T_p) - \boldsymbol{W}\boldsymbol{c}] + \tilde{\boldsymbol{n}}. \tag{10}$$

With Eq. (10), the CL estimation problem is to estimate the parameter γ, with nuisance parameters T_p and $\boldsymbol{c}$.

3 Physical Mechanisms for CL Estimation

The radiance model [Eq. (10)] becomes nonidentifiable in the important limit of an optically thin plume and spectrally flat background of temperature T_b, given by $\boldsymbol{L}_b = \boldsymbol{B}(T_b)$. The significance of this limit is that the LWIR spectra of many natural backgrounds are quite smooth, as compared to those of chemical vapors, and can therefore be approximated as blackbodies. Indeed, this approximation forms the basis for many gas detection algorithms.[12] Due to this nonidentifiability, the reliable recovery of the CL parameter can be problematic, and we must identify and exploit physical mechanisms that avoid this situation, which we accomplish by careful analysis of the radiance model.

The background model [Eq. (8)] accommodates the flat background scenario by the choice of coefficients $\boldsymbol{c} = \boldsymbol{c}(T_b)$ such that $\boldsymbol{W}\boldsymbol{c}(T_b) \simeq \boldsymbol{B}(T_b)$. The radiance model becomes

$$\boldsymbol{L}_{\text{on}}^{(\text{comp})} = \boldsymbol{B}(T_b) + \gamma(T_p - T_b)\boldsymbol{\alpha}\odot\dot{\boldsymbol{B}} + \tilde{\boldsymbol{n}}, \tag{11}$$

where $\dot{\boldsymbol{B}}(T) = d\boldsymbol{B}/dT$. Clearly, only the product $\gamma(T_p - T_b)$ may be estimated from Eq. (11), so the only way that γ may be recovered is with the use of ancillary data that yields T_p (under our assumptions, T_b may be estimated from the off-plume pixels in this scenario). This assumption underlies many CL estimation algorithms that have been proposed.[7,13,14] Indeed, if the plume can be assumed to be in thermal equilibrium with the atmosphere, then estimating $T_p = T_a$ from the image is quite feasible from atmospheric compensation algorithms. However, there are many situations in which this assumption does not hold and other mechanisms for recovering CL must be exploited.

Examining Eq. (10) reveals three additional mechanisms in addition to ancillary measurement of T_p that enable identifiability. The first is the nonlinearity of Beer's law [Eq. (7)]. The intuition behind this approach can be observed by expanding the exponential past the first order, with a flat background.

$$\boldsymbol{L}_{\text{on}}^{(\text{comp})} = \boldsymbol{B}(T_b) + (T_p - T_b)\left(\gamma\boldsymbol{\alpha} - \frac{\gamma^2}{2}\boldsymbol{\alpha}\odot\boldsymbol{\alpha}\right)\odot\dot{\boldsymbol{B}} + \tilde{\boldsymbol{n}}. \tag{12}$$

Linear regression on Eq. (12) will recover separate estimates of $\gamma(T_p - T_b)$ and $\gamma^2(T_p - T_b)$, allowing γ and $T_p - T_b$ to be separated. A similar result is obtained with orthogonal background suppression.[15] Nonlinear regression accomplishes the same task without the need to explicitly expand the exponential.[3,9,16]

A second mechanism for identifiability of Eq. (10) is the existence of a spectrally structured, i.e., nongraybody, background in an on-plume pixel. This mechanism applies even with a thin plume, so the nonlinearity of Beer's law need not be exploited. The radiance model with a structured background is

$$\boldsymbol{L}^{(\text{comp})} = \boldsymbol{W}\boldsymbol{c} + \gamma\boldsymbol{\alpha}\odot[\boldsymbol{B}(T_p) - \boldsymbol{W}\boldsymbol{c}] + \tilde{\boldsymbol{n}}. \tag{13}$$

The existence of the structured background $\boldsymbol{W}\boldsymbol{c}$ in Eq. (13) allows recovery of all parameters γ, T_p, and c by nonlinear regression, in principle. However, this approach depends on sufficient overlap in the spectral structures of the gas signature $\boldsymbol{\alpha}$ and the background $\boldsymbol{W}\boldsymbol{c}$.

The previous mechanisms for CL estimation can operate with a single pixel. A fourth approach[7] relies on the exploitation of spatial structure in a scene and enables CL estimation even in the flat background, thin plume limit with no prior knowledge of T_p. The crucial ingredient is spatial variation of the background radiance, which is manifested as spatial variation of background temperature $T_b = T_b(x)$ in the flat background limit, where x represents a position in the image. The radiance model is

$$\boldsymbol{L}^{(\text{comp})}(x) = \boldsymbol{B}(T_b, x) + \gamma[T_p - T_b(x)]\boldsymbol{\alpha}\odot\dot{\boldsymbol{B}} + \tilde{\boldsymbol{n}}(x). \tag{14}$$

From Eq. (14), independent estimates of

$$u(x) = T_b(x) \quad v(x) = \gamma[T_p - T_b(x)] \tag{15}$$

may be estimated. If $T_b(x)$ varies with x, then the linear relationship exhibited in Eq. (15) allows the recovery of γ as the slope. A crucial assumption on which this approach rests is that γ is constant over the region of application, in which sufficient background radiance variability occurs.

Each of the various mechanisms that have been identified as enabling CL estimation may be present in a given scene, individually or in concert, to a greater or lesser degree depending on the local environment, plume composition, and sensor. A crucial question for sensor and system design, and for analysis of potential system utility, is the potential

performance limits of CL estimation algorithms. This question will be addressed in the next section through the use of Cramer-Rao lower bounds on the variance of estimators for CL. These bounds provide limits of performance that include all physical mechanisms present in the radiance model [Eq. (10)], but are independent of the specific algorithm that may be employed. The bounds therefore provide a guide to the potential noise-limited performance, and specific algorithms may be evaluated on the basis of how closely they approach the bounds.

4 Algorithm Performance Limits

4.1 *Cramer-Rao Bounds*

The compensated radiance model for a single pixel [Eq. (5)] has the form

$$\boldsymbol{L}^{(\mathrm{comp})}(\boldsymbol{\theta}) = \boldsymbol{\mu}(\boldsymbol{\theta}) + \tilde{\boldsymbol{n}}, \tag{16}$$

where the parameter vector $\boldsymbol{\theta} = (T_p, \gamma, \boldsymbol{c})$, and

$$\boldsymbol{\mu}(\boldsymbol{\theta}) = \boldsymbol{B}(T_p) + \boldsymbol{\tau}_p(\gamma) \odot [\boldsymbol{W}\boldsymbol{c} - \boldsymbol{B}(T_p)] + \tilde{\boldsymbol{n}}. \tag{17}$$

We model the sensor noise term $\tilde{\boldsymbol{n}} = \boldsymbol{n}/\boldsymbol{\tau}_a$ as a zero mean Gaussian random vector. Below, we will estimate the covariance $\boldsymbol{C}_{\tilde{\boldsymbol{n}}}$ of this vector from the observed data. We will further approximate this covariance as independent of the parameter vector $\boldsymbol{\theta}$, so the Fisher information matrix is given by

$$\mathbf{I}(\theta)_{i,j} = \left(\frac{\partial \boldsymbol{\mu}}{\partial \boldsymbol{\theta}_i}\right)^T \boldsymbol{C}_{\tilde{\boldsymbol{n}}}^{-1} \left(\frac{\partial \boldsymbol{\mu}}{\partial \boldsymbol{\theta}_j}\right), \tag{18}$$

and the Cramer-Rao lower bound for the covariance $\boldsymbol{C}_{\hat{\theta}}$ of any estimator $\hat{\boldsymbol{\theta}}$ for $\boldsymbol{\theta}$ is[17]

$$\boldsymbol{C}_{\hat{\theta}} - \boldsymbol{I}^{-1}(\boldsymbol{\theta}) \geq 0, \tag{19}$$

where the meaning of the inequality is that the matrix on the LHS is positive definite. In particular, the variances of the parameter estimates are bounded below by

$$\mathrm{Var}(\hat{\theta}_i) \geq [\boldsymbol{I}^{-1}(\boldsymbol{\theta})]_{i,i}. \tag{20}$$

The case of multiple pixels requires a model for spatial variation of the radiance. We will adopt a spatial temperature gradient imposed on a spatially invariant background of smooth, but otherwise arbitrary, emissivity. This situation can be incorporated into the linear model [Eq. (8)] by adding a spatial gradient to the coefficients $\boldsymbol{c}$.

$$\boldsymbol{c}(x) = \boldsymbol{c}^{(0)} + \delta x \boldsymbol{c}^{(1)}, \tag{21}$$

where x indexes the position in the image along the direction parallel to the temperature gradient. In order to obtain the interpretation $\delta = \partial T_b/\partial x$, we choose $\boldsymbol{c}^{(1)}$ to be the least squares solution to

$$\boldsymbol{B}(T_b) \odot (\boldsymbol{W}\boldsymbol{c}^{(1)}) = \dot{\boldsymbol{B}}(T_b) \odot (\boldsymbol{W}\boldsymbol{c}^{(0)}), \tag{22}$$

which results in the following linear relationship between $\boldsymbol{c}^{(1)}$ and $\boldsymbol{c}^{(0)}$.

$$\boldsymbol{c}^{(1)} = \boldsymbol{A}\boldsymbol{c}^{(0)}$$

$$\boldsymbol{A} = (\boldsymbol{W}^T\mathbf{W})^{-1}\boldsymbol{W}^T \left\{ \left[\frac{\dot{\boldsymbol{B}}(T_b)}{\boldsymbol{B}(T_b)} \otimes \mathbf{1}^{(N_{\mathrm{pix}})}\right] \odot \boldsymbol{W} \right\}.$$

The compensated radiance $\boldsymbol{L}^{(N_{\mathrm{pix}},\mathrm{comp})}$ of N_{pix} pixels may be arranged as the columns of an $N_{\mathrm{band}} \times N_{\mathrm{pix}}$ matrix, given by

$$\boldsymbol{L}^{(N_{\mathrm{pix}},\mathrm{comp})}(\boldsymbol{\theta}) = \boldsymbol{\mu}^{(N_{\mathrm{pix}})}(\boldsymbol{\theta}) + \tilde{\boldsymbol{n}}^{(N_{\mathrm{pix}})}, \tag{23}$$

where

$$\begin{aligned}\boldsymbol{\mu}^{(N_{\mathrm{pix}})}(\boldsymbol{\theta}) = \boldsymbol{B}(T_p) \otimes \mathbf{1}^{(N_{\mathrm{pix}})} + [\boldsymbol{\tau}_p(\gamma) \otimes \mathbf{1}^{(N_{\mathrm{pix}})}] \odot \{(\boldsymbol{W} \otimes \boldsymbol{I}^{(N_{\mathrm{pix}})}) \\ \times [\boldsymbol{c}^{(0)} \otimes \mathbf{1}^{(N_{\mathrm{pix}})} + (\delta \boldsymbol{A}\boldsymbol{c}^{(0)}) \otimes \boldsymbol{x}] - \boldsymbol{B}(T_p) \otimes \mathbf{1}^{(N_{\mathrm{pix}})}\}.\end{aligned} \tag{24}$$

In Eq. (24), $\boldsymbol{x}$ is the vector of x-coordinates of the pixels included, and $\mathbf{1}^{(N_{\mathrm{pix}})}$ is the N_{pix}-component vector with each component equal to unity. When analyzing the model with spatial dependence, we augment the parameter vector $\boldsymbol{\theta}^{(N_{\mathrm{pix}})} = (T_p, \gamma, \boldsymbol{c}, \delta)$ to include the background temperature gradient δ. The noise is taken to be independent across pixels.

We may compute the Cramer-Rao bound [Eq. (19)] with knowledge of the sensor noise covariance $\boldsymbol{C}_{\tilde{\boldsymbol{n}}}$ and the partial derivatives.

$$\frac{\partial \boldsymbol{\mu}^{(N_{\mathrm{pix}})}}{\partial T_p} = \{\dot{\boldsymbol{B}}(T_b) \odot [\mathbf{1} - \boldsymbol{\tau}_p(\gamma)]\} \otimes \mathbf{1}^{(N_{\mathrm{pix}})}$$

$$\begin{aligned}\frac{\partial \boldsymbol{\mu}^{(N_{\mathrm{pix}})}}{\partial \gamma} = \dot{\boldsymbol{\tau}}_p(\gamma) \odot [\boldsymbol{W}\boldsymbol{c}^{(0)} - \boldsymbol{B}(T_p)] \otimes \mathbf{1}^{(N_{\mathrm{pix}})} \\ + [\dot{\boldsymbol{\tau}}_p(\gamma) \odot \boldsymbol{W}\boldsymbol{c}^{(1)}] \otimes (\delta \boldsymbol{x})\end{aligned}$$

$$\frac{\partial \boldsymbol{\mu}^{(N_{\mathrm{pix}})}}{\partial c_i^{(0)}} = [\boldsymbol{\tau}_p(\gamma) \otimes \mathbf{1}^{(N_{\mathrm{pix}})}] \odot (\boldsymbol{W}_i \otimes \mathbf{1}^{(N_{\mathrm{pix}})} + \delta \boldsymbol{W}\boldsymbol{A}_i \otimes \boldsymbol{x})$$

$$\frac{\partial \boldsymbol{\mu}^{(N_{\mathrm{pix}})}}{\partial \delta} = [\boldsymbol{\tau}_p(\gamma) \odot (\boldsymbol{W}\boldsymbol{c}^{(1)})] \otimes \boldsymbol{x},$$

where, for a matrix $\boldsymbol{M}$, the notation $\boldsymbol{M}_i$ refers to the i'th column. We may estimate the noise covariance in a variety of ways. A sensor noise model[18,19] may be employed based on the characteristics of the instrument components and scene under test. For existing sensors, the noise covariance may be estimated from a scene, ideally by the placement of a blackbody calibration target within the sensor field of view.[2] In this paper, we estimate $\boldsymbol{C}_{\tilde{\boldsymbol{n}}}$ from a measured scene from the Telops FIRST sensor[2] that contains broad regions of homogeneous sky background. Since there is little spatial variation in such regions, subtracting the local mean radiance from a sample of such pixels gives an estimate of the sensor noise.

4.2 *Results*

We will illustrate the utility of the CR bounds in Sec. 4.2.1 with a series of examples based on simulated, idealized

background materials. In Sec. 4.2.2, we will expand our analysis to include measured emissivities of a variety of naturally occurring materials. Throughout, we choose the columns of the model matrix $\boldsymbol{W}$ from Eq. (8) to consist of a basis of linear B-splines, with the dimension $N_{\text{basis}} = 24$ chosen so that the natural emissivities considered can be well approximated.

4.2.1 *Simulated background emissivities*

Our first example will be a scene with a spatially constant blackbody background at constant temperature T_b, chosen to be 294 K. The radiance model [Eq. (10)] is employed with background coefficients $\boldsymbol{c}$ chosen to obey $\boldsymbol{W}\boldsymbol{c} \simeq \boldsymbol{B}(T_b)$. Figure 2(a) displays the square root of the Cramer-Rao lower bound on the variance of the CL estimate, $\sqrt{\text{Var}(\hat{\gamma})}$, as a function of plume temperature, T_p, and CL, γ. Two cuts through this surface at two different constant plume temperatures are shown in Fig. 2(b). Recalling Eq. (11), the radiance model becomes nonidentifiable in the thin-plume limit, which is manifested by an exploding CR bound. The bound also blows up as the plume temperature approaches that of the background, so there is no thermal contrast between the two. This behavior, too, is expected from Eq. (10) as the plume becomes invisible in this limit. Another notable feature is the minimum in the bound that occurs at moderate values of CL, for fixed T_p. CL estimation performance degrades as the plume becomes opaque. In this limit, no background radiance reaches the sensor, the plume spectral signature is washed out into that of a blackbody at the plume temperature, and differences in plume strength are no longer visible.

Ancillary measurement of plume temperature is necessary in order to estimate CL in the thin plume, flat background limit. This case is presented in Fig. 3, in which perfect knowledge of T_p is assumed. The plume gas species and

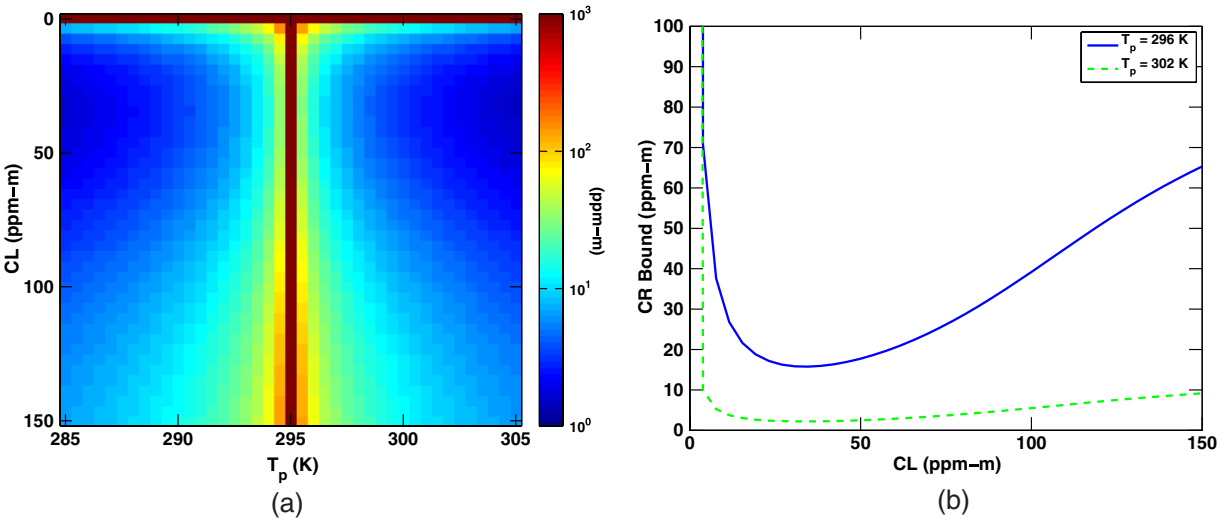

Fig. 2 Cramer-Rao lower bounds on $\sqrt{\text{Var}(\hat{\gamma})}$ for sulfur hexafluoride (SF_6) with a blackbody background (a), along with two cuts (b) at constant plume temperatures of 296 and 302 K.

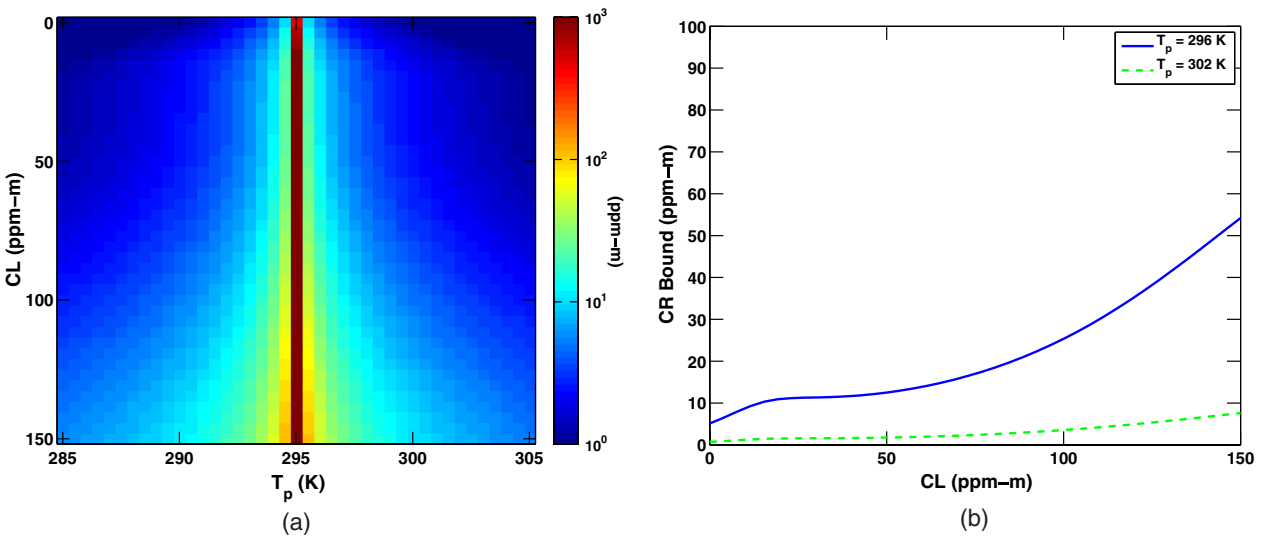

Fig. 3 Cramer-Rao lower bounds on $\sqrt{\text{Var}(\hat{\gamma})}$ for SF_6 with a blackbody background, with ancillary measurement of plume temperature (a), along with two cuts (b) at constant plume temperatures of 296 and 302 K.

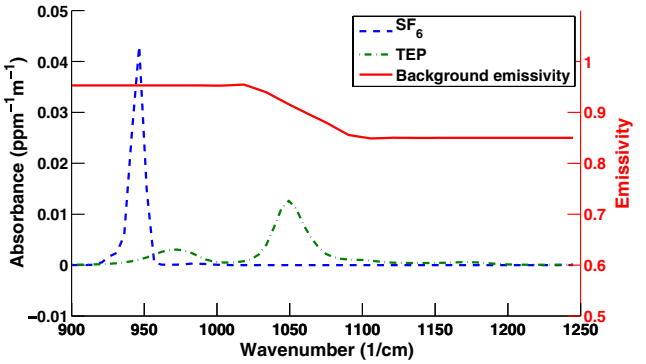

Fig. 4 Spectra used to demonstrate the effects of background emissivity on concentration-path length (CL) estimation bounds. The left hand axis applies to the absorption spectra of SF_6 (blue dashed) and triethyl phosphate (TEP) (green dashed-dotted), while the right hand axis applies to the background emissivity (red solid) assumed in the calculations.

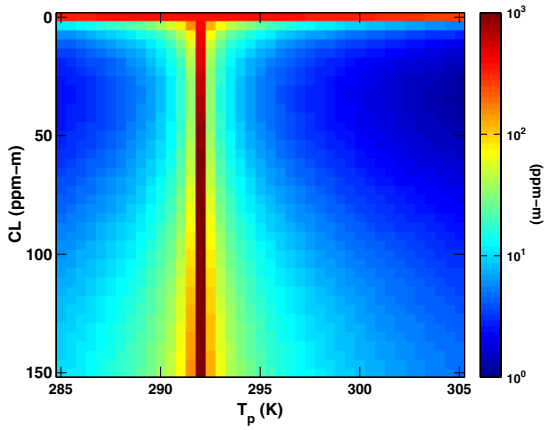

Fig. 5 Cramer-Rao lower bounds for CL estimation for SF_6 with the structured background from Fig. 4, as functions of plume temperature T_p and CL. The background temperature was taken to be 295 K.

background temperature are the same as in Fig. 2. It is evident that the additional information from the ancillary measurement eliminates the singularity in the bound in the thin plume limit and enables more accurate CL estimation at low and moderate plume strengths. As the plume strength increases, however, the nonlinearity of Beer's law becomes more important, and the additional information that knowledge of T_p imparts is not as great. In the limit of an opaque plume, of course, the ancillary measurement is of no value.

The presence of spectral structure in the background emissivity, even the relatively smooth spectra typical in the LWIR regime, can dramatically alter the prospects for CL estimation. The interplay between the spectra of the gas and the background plays an important role in this case. In order to elucidate the effects, we choose a simple piecewise linear background spectrum shown in Fig. 4, along with the absorption spectra of sulfur hexafluoride (SF_6) and triethyl phosphate (TEP). If the background spectrum is flat over the support of the gas spectrum, as is the case with SF_6, then the only effect on CL estimation is a shift in the effective background temperature if the emissivity is less than unity. This effect is demonstrated in Fig. 5, in which the CR bounds for $\hat{\gamma}$ are plotted as a function of T_p and γ for the background emissivity given in Fig. 4; the results may be compared with those of Fig. 2(a), which assumed a blackbody background. The flat emissivity of $\epsilon_b = 0.95$ over the support of the SF_6 spectrum results in an effective temperature shift of a few degrees. The situation is dramatically different when the background emissivity is not flat over the support of the gas spectrum, as is the case for TEP. In this case, as shown in Fig. 6, the singularities in the CR bound for $\hat{\gamma}$ have disappeared, and the symmetry between plume temperatures above and below that of the background has been broken. It is apparent that the spectral structure in the background enables CL estimation, even in the limits of thin plume or no plume-background temperature contrast, confirming the intuition from Eq. (12). Figure 7 shows two cuts through Fig. 6(b). We observe that the CR bounds still rise as the plume becomes opaque, as we expect,

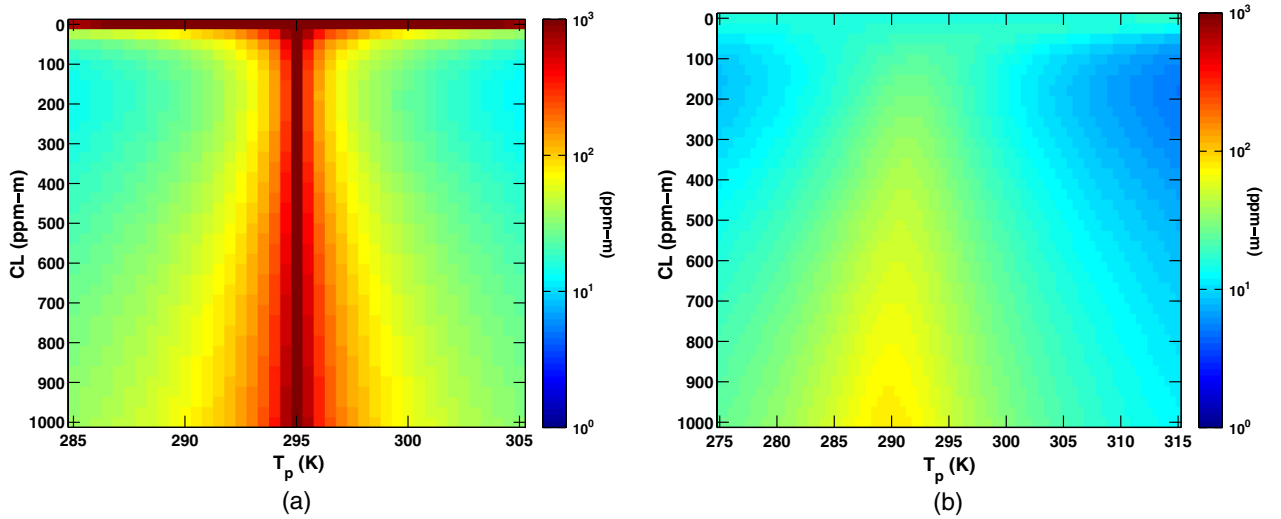

Fig. 6 Cramer-Rao lower bounds for CL estimation for TEP with a blackbody (a) and structured (b) background, both at temperature 295 K, as functions of plume temperature T_p and CL.

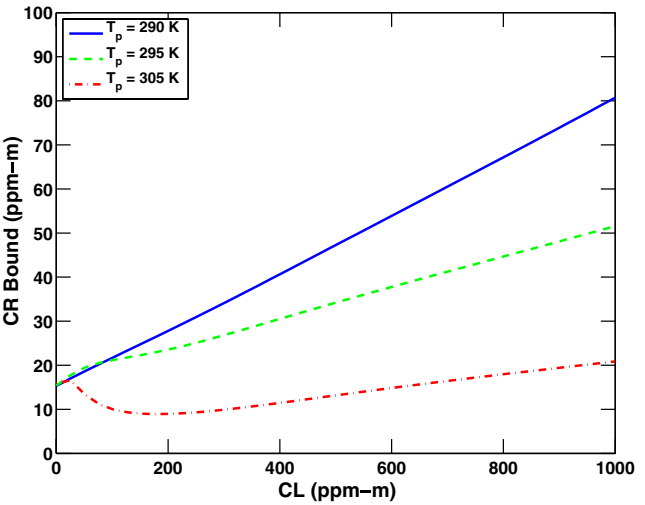

Fig. 7 Cuts at constant plume temperature through the surface of Fig. 6(b).

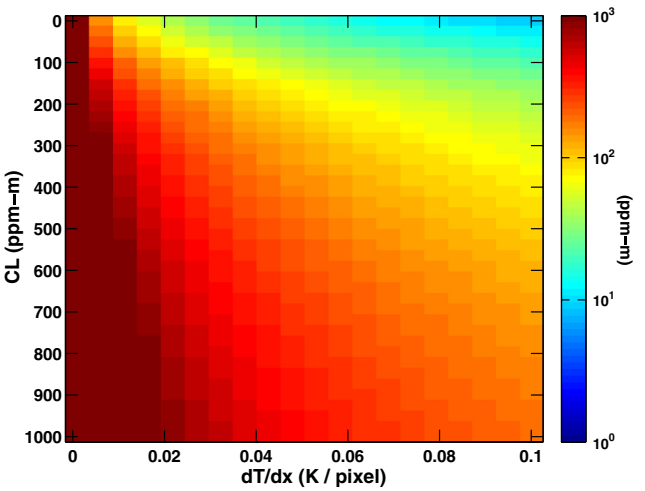

Fig. 8 Cramer-Rao lower bounds for CL estimation for TEP with a blackbody background with constant temperature gradient, as a function of CL and gradient, with no plume-background temperature contrast.

since the background cannot have influence when it is obscured by the plume.

The examples presented so far all involve CL estimation with a single on-plume pixel. We now relax this constraint and consider the benefits available with multiple pixels, assuming there is structure to the background that can be exploited. We model the case of a background with constant emissivity, but with a spatial gradient in temperature, as represented by Eq. (21). The first example we present is that of a blackbody background with temperature gradient. We estimate CL from an 8×8 pixel region, over which we assume that the plume CL is constant. Figures 8 and 9 show the CR bound for the CL estimate as a function of CL and temperature gradient, with both the absence of a plume-background temperature contrast and a contrast of 2 K at the center of the sample region. It is apparent that the temperature gradient enables CL estimation for arbitrarily thin plumes, eliminating the need for an ancillary plume temperature measurement. A plume-background temperature contrast is seen to be very helpful. For relatively small values of CL, the information available from plume nonlinearities renders the gradient information superfluous. For larger values of CL, the increasing opacity of the plume impacts the variance of the estimator, which gradient information cannot combat.

The behavior of the lower bound as a function of temperature gradient and plume temperature is shown in Fig. 10. When a spatial gradient is present, the need for a temperature contrast between the background and the plume is eliminated, although some such contrast is present due to the effect of the gradient. However, this small residual contrast can be quite small compared to that necessary for CL estimation to be accomplished via the nonlinear effect only, as can be seen from Fig. 9.

The effect of the spatial background variation acting in concert with a structured background emissivity is shown in Fig. 11. The emissivity, which is spatially constant over the 8×8 region used for estimation, is the same as that shown in Fig. 4, which has substantial overlap with the TEP gas signature. Comparing Fig. 11(a) with the blackbody case in Fig. 10, both with CL set at 20 ppm-m, we observe that even this modest amount of background spectral

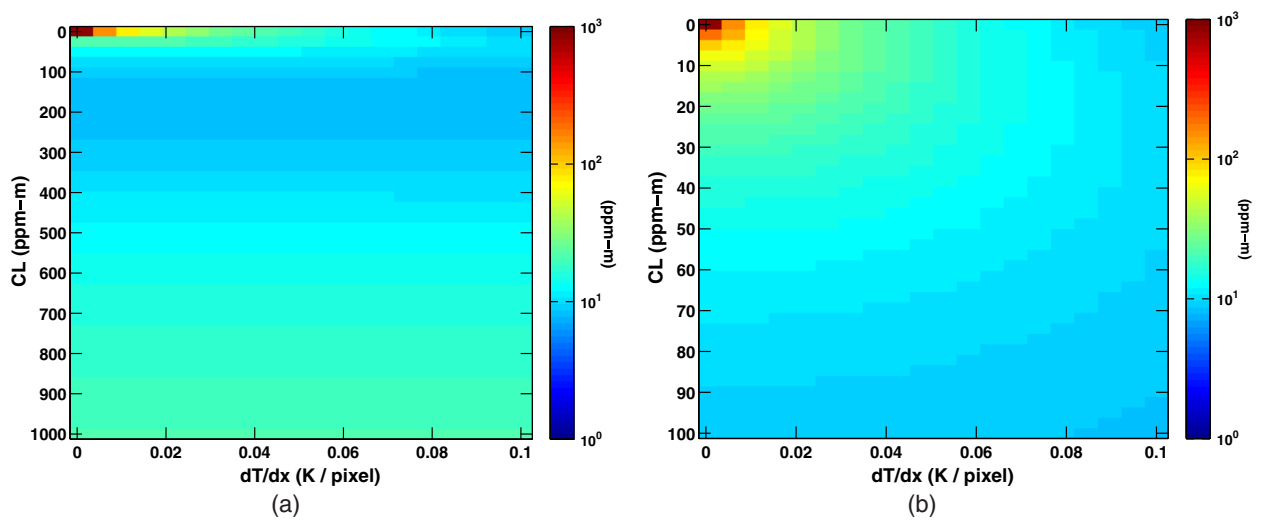

Fig. 9 Cramer-Rao lower bounds for CL estimation for TEP with a blackbody background with constant temperature gradient, as a function of CL and gradient (a), with details near origin (b). The plume-background temperature contrast is 2 K.

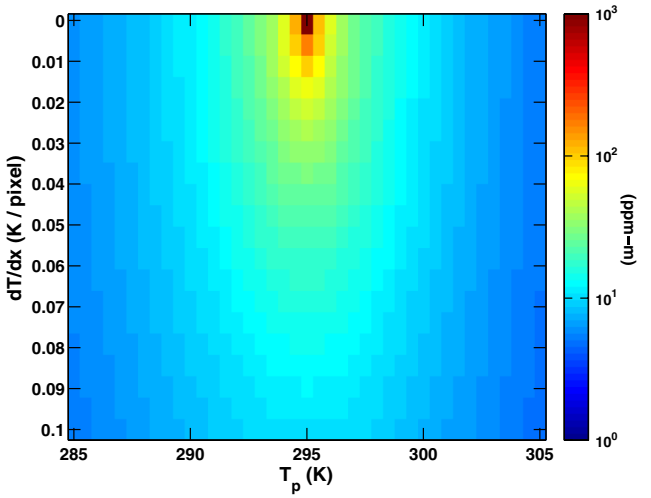

Fig. 10 Cramer-Rao lower bounds for CL estimation for TEP with a blackbody background with constant temperature gradient, as a function of gradient and plume temperature. The CL product is fixed at 20 ppm-m.

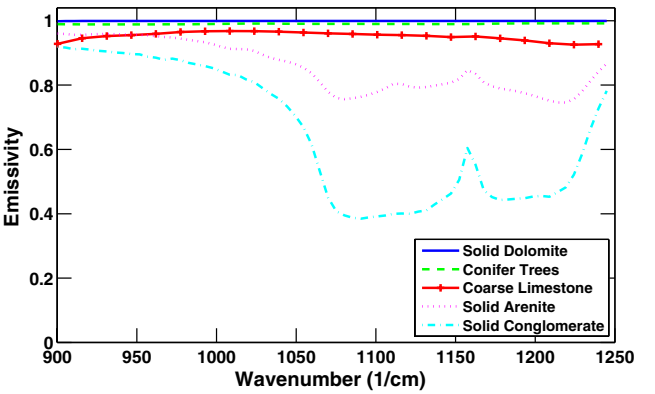

Fig. 12 Emissivities of a number of materials, drawn from the ASTER library.

structure is sufficient to render both the plume-background temperature contrast and background temperature gradient irrelevant. When the CL is raised to 100 ppm-m in Fig. 11(b), the plume-background temperature contrast begins to play a role, but the background temperature gradient is still overwhelmed by the other factors.

4.2.2 *Measured background emissivities*

An important question is whether the idealized background emissivities used in the previous section are representative of real materials. To address this issue, we present performance bounds in which the background emissivities are drawn from the ASTER library of measured spectra from real materials.[20] We have chosen a sample of five materials, shown in Fig. 12, to illustrate a range of possible behaviors. They are ordered in the degree to which they resemble a blackbody over the LWIR window; solid dolomite and conifer trees are very black in this window, while coarse limestone exhibits some spectral structure, and arenite and conglomerate rock have substantial spectral structures that overlap that of TEP absorbance.

In Fig. 13, we demonstrate that the limit of an ideal blackbody is, for all practical purposes, attained by solid dolomite over the LWIR band. The CR bounds on CL estimation with the plume temperature assumed unknown are computed for both SF_6 (a) and TEP (b). We observe that these results are almost identical with those of Figs. 2(a) and 6(a), which assumed an exact blackbody background. In addition to dolomite, there are other materials that behave similarly.

Finally, we explore the effect of a variety of natural backgrounds in Fig. 14. We have chosen TEP for this illustration as its relatively broad spectral support has substantial overlap with many background spectra. In the LWIR band, conifer trees are almost as good a blackbody as dolomite; Fig. 14(a) shows that the CR bounds are very similar to those of Fig 13(b), although small differences are apparent. In particular, the vertical ridge of high variance has shifted slightly to a lower effective temperature,due to the fact that that the trees are slightly gray, as opposed to black, and the horizontal

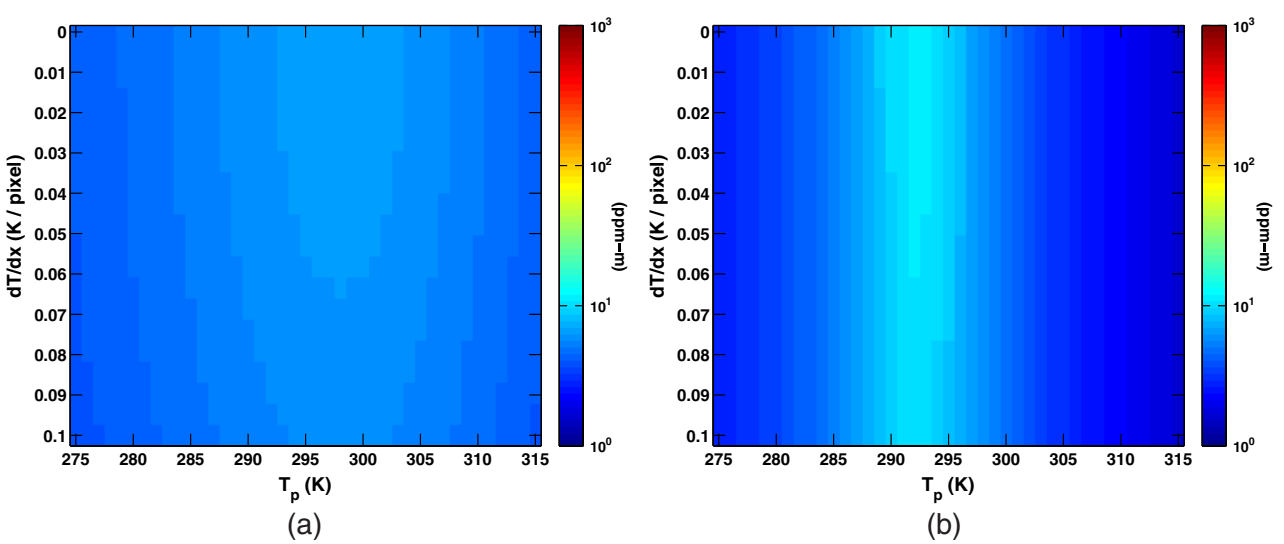

Fig. 11 Cramer-Rao lower bounds for CL estimation for TEP with the structured background emissivity of Fig. 4 and constant temperature gradient, as a function of gradient and plume temperature. The CL is set at 20 ppm-m (a) and 100 ppm-m (b).

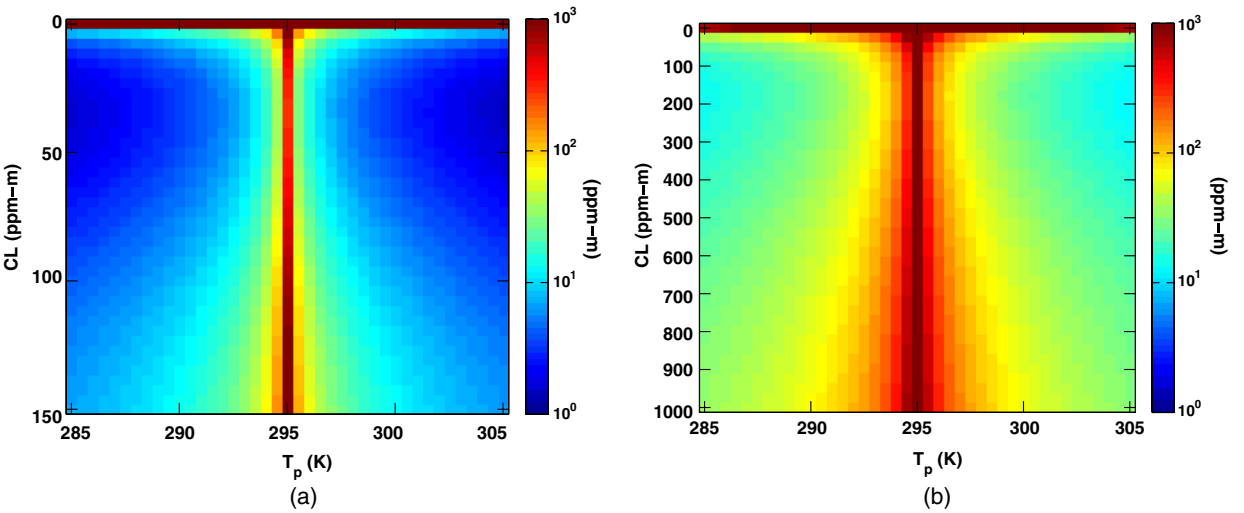

Fig. 13 Cramer-Rao lower bounds for CL estimation for SF_6 (a) and TEP (b) with the background emissivity of solid dolomite.

ridge in the limit of small CL is slightly lower due to the presence of some spectral structure. These differences are more pronounced when the background is taken to be coarse limestone, in Fig. 14(b). The presence of strong spectral structure in the background, as in arenite, gives rise to a very different pattern in the bounds, as seen in Fig. 14(c). This pattern is similar to that resulting from the simulated background of Fig. 6(b). An even more pronounced spectral structure in the emissivity, such as with conglomerate, results in further improvements in the CR bounds, as seen

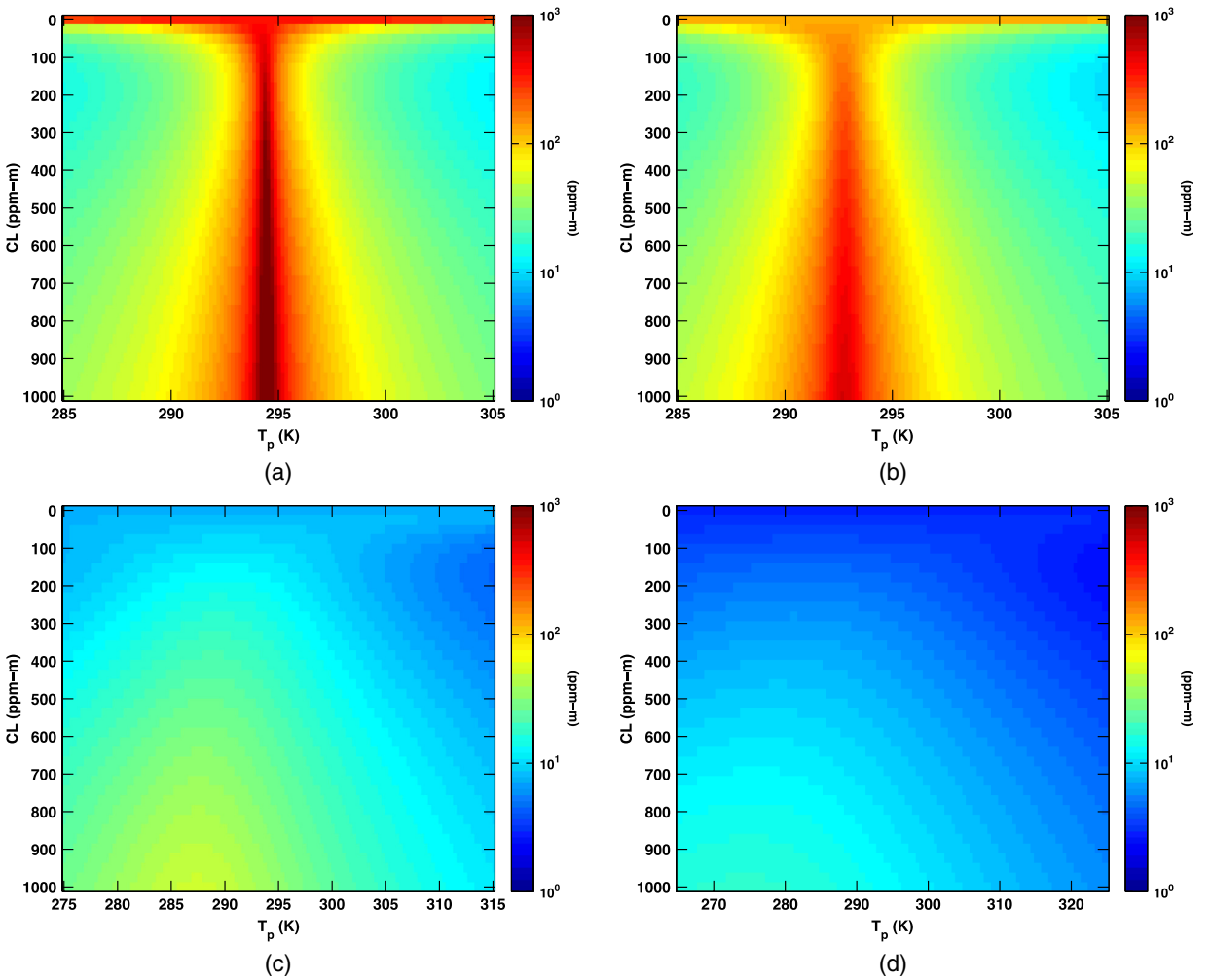

Fig. 14 Cramer-Rao lower bounds for CL estimation for TEP with background emissivities of conifer trees (a), coarse limestone (b), solid arenite (c), and solid conglomerate (d).

in Fig. 14(d). Between Figs. 13 and 14, we may conclude that the two simulated background emissivities considered in Sec. 4.2.1 are representative of the behaviors seen with natural backgrounds, although the range of possibilities is wide.

5 Conclusion

The mean CL is the central parameter to be estimated to accomplish remote quantification of gaseous plumes. The recovery of this parameter from hyperspectral data is not a simple task, however, due to the complex, nonlinear way it interacts with the rest of the scene, and due to the nonidentifiability of the radiance model in the most common limit, that of a thin plume with spectrally flat background. The purpose of this paper was twofold: to separate the various physical effects that may be exploited in order to estimate CL and to obtain quantitative bounds on the quality of such estimates that are independent of the specific algorithms employed. These results are of great importance for the design and assessment of both sensor systems and of estimation algorithms. They enable the system designer to place reasonable specifications on the sensor parameters, taking into account the intended deployment scenario and gas species of interest. The separation of the physical effects that enable CL estimation allows the algorithm developer to quantitatively choose which effects will be most profitable to exploit. Finally, an operational system may be assessed by comparing experimental quantification results with the theoretical bounds that were derived here.

Acknowledgments

This work is sponsored by the Defense Threat Reduction Agency under Air Force Contract FA8721-05-C-0002. Opinions, interpretations, conclusions, and recommendations are those of the authors and not necessarily endorsed by the U. S. Government.

References

1. D. W. Warren, J. A. Hackwell, and D. J. Gutierrez, "Compact prism spectrographs based on aplanatic principles," *Opt. Eng.* **36**(4), 1174–1182 (1997).
2. V. Farley et al., "Performance of the FIRST: a long-wave infrared hyperspectral imaging sensor," *Proc. SPIE* **6398**, 63980T (2006).
3. R. Harig, G. Matz, and P. Rusch, "Scanning infrared remote sensing system for identification, visualization, and quantification of airborne pollutants," *Proc. SPIE* **4574**, 83–94 (2002).
4. D. Flanigan, "Prediction of the limits of detection of hazardous vapors by passive infrared with the use of MODTRAN," *Appl. Opt.* **35**(30), 6090–6098 (1996).
5. T. Burr and N. Hegarther, "Overview of physical models and statistical approaches for weak gaseous plume detection using passive infrared hyperspectral imagery," *Sensors* **6**(12), 1721–1750 (2006).
6. G. E. Thomas and K. Stamnes, *Radiative Transfer in the Atmosphere and Ocean*, Cambridge University Press, Cambridge, UK (2002).
7. S. J. Young, "Detection and quantification of gases in industrial-stack plumes using thermal-infrared hyperspectral imaging," Aerospace Report ATR-2002(8407)-1, The Aerospace Corporation (2002).
8. S. J. Young, B. R. Johnson, and J. A. Hackwell, "An in-scene method for atmospheric compensation of thermal hyperspectral data," *J. Geophys. Res.: Atmos.* **107**(D24), 4774 (2002).
9. C. M. Gittins, "Detection and characterization of chemical vapor fugitive emissions by nonlinear optimal estimation: theory and simulation," *Appl. Opt.* **48**(23), 4545–4561 (2009).
10. R. M. Goody and Y. L. Yung, *Atmospheric Radiation: Theoretical Basis*, Oxford University Press, USA (1995).
11. S. W. Sharpe et al., "Gas-phase databases for quantitative infrared spectroscopy," *Appl. Spectrosc.* **58**(12), 1452–1461 (2004).
12. D. G. Manolakis and F. M. D'Amico, "A taxonomy of algorithms for chemical vapor detection with hyperspectral imaging spectroscopy," *Proc. SPIE* **5795**, 125–133 (2005).
13. A. Hayden, E. Niple, and B. Boyce, "Determination of trace-gas amounts in plumes by the use of orthogonal digital filtering of thermal-emission spectra," *Appl. Opt.* **35**(16), 2802–2809 (1996).
14. N. B. Gallagher, B. M. Wise, and D. M. Sheen, "Estimation of trace vapor concentration-pathlength in plumes for remote sensing applications from hyperspectral images," *Anal. Chim. Acta* **490**(1–2), 139–152 (2003).
15. A. Hayden and R. Noll, "Remote trace gas quantification using thermal IR spectroscopy and digital filtering based on principal components of background scene clutter," *Proc. SPIE* **3071**, 158–168 (1997).
16. P. Tremblay et al., "Standoff gas identification and quantification from turbulent stack plumes with an imaging Fourier-transform spectrometer," *Proc. SPIE* **7673**, 76730H (2010).
17. S. M. Kay, *Fundamentals of Statistical Signal Processing: Estimation Theory*, Prentice-Hall Inc., Upper Saddle River, New Jersey (1993).
18. E. T. Scharlemann, "Modeling chemical detection sensitivities of active and passive remote sensing systems," *Proc. SPIE* **5154**, 126–137 (2003).
19. R. Keller and T. Lomheim, "Imaging Fourier transform spectrometer (IFTS): parametric sensitivity analysis," *Proc. SPIE* **5806**, 267–287 (2005).
20. A. Baldridge et al., "The ASTER spectral library version 2.0," *Remote Sens. Environ.* **113**(4), 711–715 (2009).

Steven E. Golowich is a technical staff member at MIT Lincoln Laboratory, where his research interests include statistical signal processing, hyperspectral imaging, synthetic aperture radar, and structured light. He was awarded a PhD degree in physics by Harvard University and an AB degree in physics and mathematics by Cornell University. Previously, he was a member of technical staff at the Bell Labs Mathematical Sciences Research Center and taught at Princeton University. He is a recipient of the American Statistical Association Outstanding Application award and the Wilcoxon Prize.

Dimitris G. Manolakis received his BS in physics and PhD in electrical engineering from the University of Athens, Greece. He is currently a senior staff member at MIT Lincoln Laboratory, Lexington, Massachusetts. Previously, he was a principal member, research staff, at Riverside Research Institute. He has taught at the University of Athens, Northeastern University, Boston College, and Worcester Polytechnic Institute. He is a coauthor of the textbooks *Digital Signal Processing: Principles, Algorithms, and Applications* (Prentice-Hall, 2006, 4th ed.), *Statistical and Adaptive Signal Processing* (Artech House, 2005), and *Applied Digital Signal Processing* (Cambridge University Press, 2011). His research experience and interests include the areas of digital signal processing, adaptive filtering, array processing, pattern recognition, remote sensing, and radar systems.